Vol.19, e190006 (2022)
doi: 10.2142/biophysico.bppb-v19.0006

Biophysics and Physicobiology
https://www.jstage.jst.go.jp/browse/biophysico/

Review Article (Invited)

Quantitative and kinetic single-molecule analysis of DNA unwinding by *Escherichia coli* UvrD helicase

Hiroaki Yokota

The Graduate School for the Creation of New Photonics Industries, Hamamatsu, Shizuoka 431-1202, Japan

Received November 29, 2021; Accepted March 7, 2022;
Released online in J-STAGE as advance publication March 10, 2022
Edited by Akihiko Ishijima

Helicases are nucleic acid-unwinding enzymes involved in the maintenance of genome integrity. Helicases share several "helicase motifs" that are highly conserved amino acid sequences and are classified into six superfamilies (SFs). The helicase SFs are further grouped into two classes based on their functional units. One class that includes SFs 3–6 functions as a hexamer that can form a ring around DNA. Another class that includes SFs 1 and 2 functions in a non-hexameric form. The high homology in the primary and tertiary structures among SF1 helicases suggests that SF1 helicases have a common underlying mechanism. However, two opposing models for the functional unit, monomer and dimer models, have been proposed to explain DNA unwinding by SF1 helicases. This paper briefly describes the classification of helicase SFs and discusses the structural homology and the two opposing non-hexameric helicase models of SF1 helicases by focusing on *Escherichia coli* SF1 helicase UvrD, which plays a significant role in both nucleotide-excision repair and methyl-directed mismatch repair. This paper reviews past and recent studies on UvrD, including the author's single-molecule direct visualization of wild-type UvrD and a UvrD mutant lacking the C-terminal 40 amino acids (UvrDΔ40C), the latter of which was used in genetic and biochemical assays that supported the monomer model. The visualization revealed that multiple UvrDΔ40C molecules jointly unwind DNA, presumably in an oligomeric form, similar to wild-type UvrD. Therefore, single-molecule direct visualization of nucleic acid-binding proteins can provide quantitative and kinetic information to reveal their fundamental mechanisms.

Key words: protein–nucleic acid interactions, protein assembly, protein oligomerization, enzyme function, fluorescence microscopy

Significance

Helicases are nucleic acid-unwinding enzymes involved in the maintenance of genome integrity. Despite the high structural homology among superfamily 1 non-hexameric helicases, two opposing models have been proposed for their functional units: monomeric and dimeric-helicase models. This paper reviews past and recent studies on the *Escherichia coli* SF1 helicase UvrD. The author's single-molecule direct visualization of a UvrD mutant lacking the C-terminal 40 amino acids (UvrDΔ40C), which was used to propose the monomer model, provided evidence for the dimer model. Thus, single-molecule direct visualization of nucleic acid-binding proteins can provide quantitative and kinetic information to reveal their fundamental mechanisms.

Corresponding author: Hiroaki Yokota, The Graduate School for the Creation of New Photonics Industries, 1955-1, Kurematsu-cho, Nishi-ku, Hamamatsu, Shizuoka 431-1202, Japan. ORCID iD: https://orcid.org/0000-0002-3435-9121, e-mail: yokota@gpi.ac.jp

Introduction

DNA replication, repair, and recombination are important mechanisms that ensure the genetic continuity of a species. In particular, maintaining genome stability requires not only rigorous DNA replication mechanisms, but also DNA repair mechanisms that are necessary to maintain genome stability. The DNA repair mechanisms remove damaged nucleotides and mismatches that constantly occur in DNA, and are highly conserved in prokaryotes and eukaryotes [1]. Consequently, their deficiency causes various diseases, such as cancer, neurodegeneration, and premature aging.

A number of proteins involved in the DNA repair mechanisms have been identified and subjected to structural analysis, and models for these mechanisms have been proposed based on detailed biochemical studies. However, since it is difficult to understand the tertiary structures and dynamic features of these complexes consisting of many subunits, it remains unclear how these molecules interact with each other and function as protein complexes.

This paper describes the classification of helicase superfamilies (SFs) and discusses the structural homology and two opposing non-hexameric helicase models for SF1 helicases by focusing on *Escherichia coli* (*E. coli*) SF1 helicase UvrD, which plays a significant role in both nucleotide-excision repair and methyl-directed mismatch repair. This paper is an extended version of the Japanese article [2] and reviews past and recent studies on UvrD, including the author's single-molecule direct visualization of wild-type UvrD and a UvrD mutant lacking the C-terminal 40 amino acids (UvrDΔ40C), the latter of which was used in genetic and biochemical assays that supported a monomer model. The visualization revealed that multiple UvrDΔ40C molecules jointly unwind DNA, most likely in an oligomeric form, similar to wild-type UvrD. Therefore, single-molecule direct visualization of nucleic acid-binding proteins can provide quantitative and kinetic information to reveal their fundamental mechanisms.

Helicase Superfamilies

Helicases are enzymes that unwind double-stranded DNA (dsDNA) into single-stranded DNA (ssDNA) using the energy derived from nucleotide hydrolysis. They are involved in DNA metabolism, including DNA replication, repair, and recombination, and are highly conserved from prokaryotes to eukaryotes.

Helicases share similar amino acid sequences in several regions, and these highly conserved sequences are called "helicase motifs" [3]. The primary structure of these motifs underlies the classification of helicases into six SFs (Table 1). In addition, the six SFs can be categorized according to the number of molecules involved in helicase functions. SF3-6 helicases that encircle DNA to form a ring structure function in a hexameric form [4,5], and SF1 and SF2 helicases function in a non-hexameric form.

Superfamily 1 (SF1) Helicases

SF1 helicases share seven helicase motifs (I, Ia, II, III, IV, V, and VI) [3], and they are further divided into three subfamilies based on primary structure analyses (UvrD/Rep-like, Pif1-like, and Upf1-like subfamilies) [6] (Table 2). SF1 helicases are also characterized by their direction of duplex unwinding. SF1A helicases have 3′→5′ polarity, whereas SF1B helicases have 5′→3′ polarity. The UvrD/Rep-like subfamily members are almost always SF1A DNA helicases, whereas those of the Pif1- and Upf1-like subfamilies are SF1B enzymes that can act on both DNA and RNA [7].

Superfamily 1 (SF1) helicases are probably the most structurally analyzed. Figure 1 shows the tertiary structures solved for SF1 helicases complexed with DNA. For the UvrD/Rep-like subfamily helicases, X-ray crystal structures were produced for UvrD [8,9] (Fig. 1A), Rep [10] (Fig. 1B) from *E. coli*, and PcrA [11] (Fig. 1C) from the thermophilic bacterium *Bacillus stearothermophilus* (*B. stearothermophilus*). These helicases have high primary structure homology (~40%) and are composed of four structural domains (1A, 1B, 2A, and 2B) and a C-terminal region, which are indicated by different colors. The structures also show similarity in their tertiary structures. The structural similarity can also be seen in other subfamilies, such as Pif1-like helicases (*E.coli* TraI [12] (Fig. 1D), *Saccharomyces cerevisiae* (*S. cerevisiae*) Pif1 [13] (Fig. 1E), and phage T4 Dda [14] (Fig. 1F)) and Upf1-like helicases (human Upf1 [15] (Fig. 1G) and *S. cerevisiae* Upf1 [15] (Fig. 1H)).

Table 1 Helicase superfamilies (SFs) and their functional units

SF	Helicase	Functional unit
SF1	UvrD, Rep, PcrA, TraI, Pif1, Dda, Upf1	Non-hexamer
SF2	RecQ, NS3, WRN	
SF3	E1	Hexamer
SF4	DnaB, gp4	
SF5	Rho	
SF6	MCM, RuvB	

Table 2 Unwinding characteristics and cellular functions of some SF1 helicases and the proposed models of their functional units

SF	Sub family	Helicase	Organism	Molecular weight (kDa)	Direction of duplex unwinding	Unwinding rate (bp/s)	Processivity (bp)	Cellular functions	Proposed models for functional unit	References
1A	UvrD/ Rep	UvrD	*E. coli*	82	3′→5′	250	240	DNA repair	Monomer/ Dimer	[8,16–23]
		Rep	*E. coli*	77	3′→5′	45	30	DNA replication	Dimer	[10,24,25]
		PcrA	*B. stearotherm ophilus*	82	3′→5′	31	5.5	DNA repair Rolling replication of plasmids	Monomer/ Dimer	[11,26,27]
1B	Pif1-like	TraI	*E. coli*	192	5′→3′	1120	> 850	DNA transfer during conjugation	Monomer/ Dimer	[12,28]
		Pif1	*S. cerevisiae*	98	5′→3′	75	10	Mitochondrial DNA maintenance	Monomer	[29]
		Dda	phage T4	50	5′→3′	262	64	DNA replication initiation DNA recombination	Monomer	[30,31]
1B	Upf1-like	Upf1	*H. sapiens*	124	5′→3′	0.162, 0.32 0.19 (RNA)	$> 10^4$	Telomere maintenance mRNA decay	Monomer	[32–34]
		Upf1	*S. cerevisiae*	109	5′→3′	10.2	$> 10^4$		Monomer	[34]

Dimer and Monomer Models Proposed for SF1 Helicases

Despite the high structural homology among SF1 helicases, two opposing models have been proposed: dimeric-helicase and monomeric-helicase models. The dimer model has been proposed for *E. coli* UvrD [16–22], Rep [10,24,25], and TraI [12] helicases, and *B. stearothermophilus* PcrA [26] helicase. The monomer model has also been proposed for UvrD [8,23], PcrA [11,27], TraI [28], *S. cerevisiae* Pif1 [29], phage T4 Dda [30,31], human Upf1 [32-34], and *S. cerevisiae* Upf1[34]. Table 2 lists the unwinding characteristics, cellular functions of some SF1 helicases, and the proposed models for their functional units.

These models have been proposed mainly by structural and biochemical studies, including X-ray crystallography, size-exclusion chromatography, analytical ultracentrifugation, ATPase assays, DNA-binding assays, and stopped-flow method-based single- and multiple-turnover DNA-unwinding assays. The models were investigated for some SF1 helicases using single-molecule measurements, as presented in the following sections.

Dimer Model Proposed for Wild-type UvrD

The SF1A UvrD (720 amino acids, molecular mass = 82 kDa) consisting of 1A (amino acids 1–89 and 215–280), 1B (90–214), 2A (281–377 and 551–647), and 2B (378–550) domains [8], and an unstructured C-terminal region (645–720) [35] (Figure 1A) binds to the ssDNA/dsDNA junction with high affinity and unwinds dsDNA in the 3′→5′ direction using energy derived from adenosine triphosphate (ATP) hydrolysis (Table 2). This helicase plays a crucial role in both nucleotide-excision repair and methyl-directed mismatch repair [36]. Data from past biochemical studies have indicated that wild-type UvrD exhibits optimal DNA unwinding activity in its oligomeric form (Table 3). Maluf et al. proposed a dimeric model based on the result that DNA is efficiently unwound when the [UvrD]/[DNA] ratio is greater than or equal

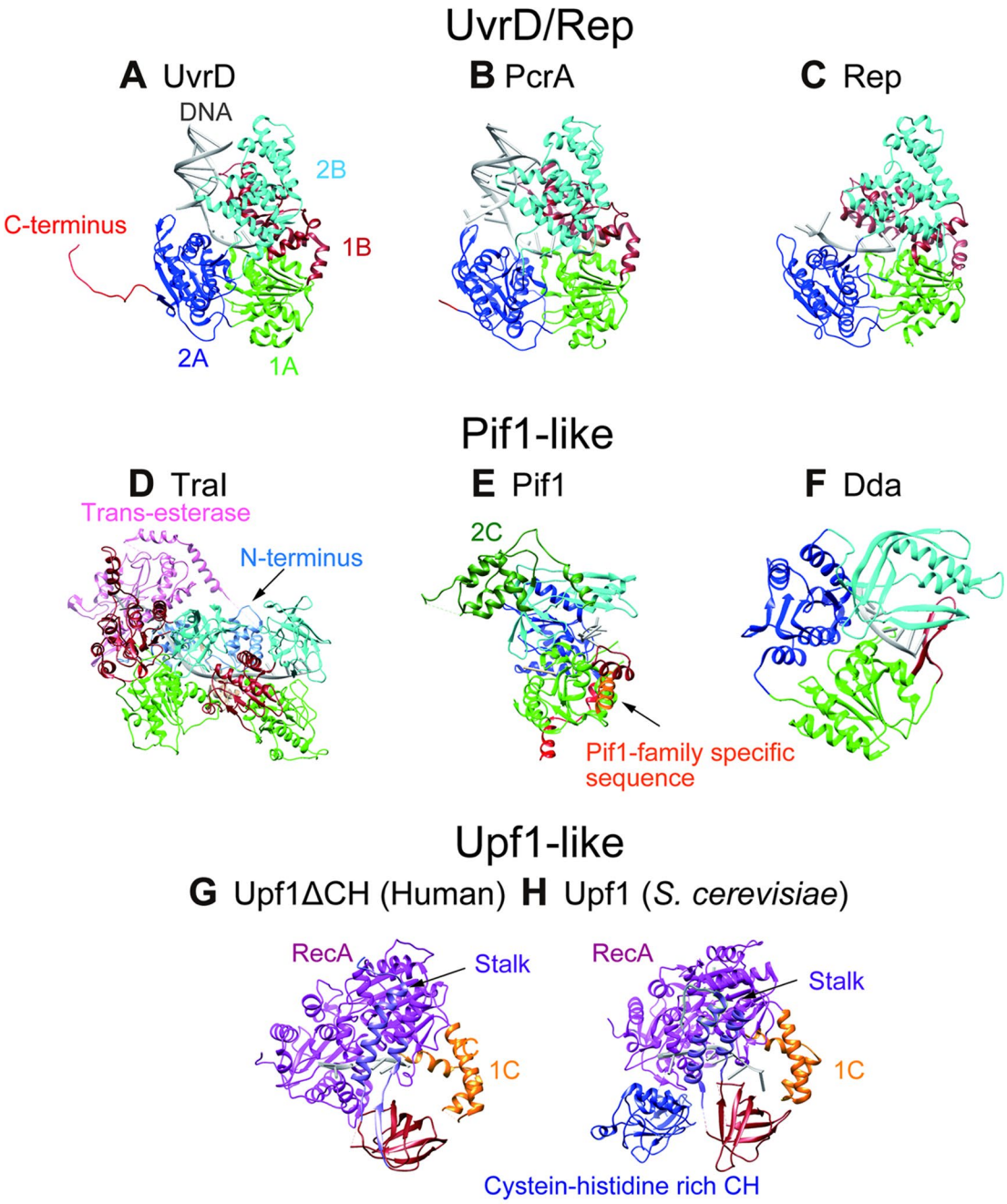

Figure 1 Tertiary structures of representative SF1 helicases. UvrD/Rep subfamily helicases. (A) *Escherichia coli* (*E. coli*) UvrD [PDB ID: 2is4], (B) *Bacillus stearothermophilus* (*B. stearothermophilus*) PcrA [PDB ID: 3pjr], and (C) *E. coli* Rep [PDB ID: 1uaa]. Pif1-like subfamily helicases: (D) *E.coli* TraI [PDB ID: 5n8o], (E) *Saccharomyces cerevisiae* (*S. cerevisiae*) Pif1 [PDB ID: 5o6d], and (F) phage T4 Dda [PDB ID: 3upu]. Upf1-like subfamily: (G) human Upf1 ΔCH that lacks the cysteine-histidine-rich CH domain [PDB ID: 2xzo] and (H) *S. cerevisiae* Upf1 [PDB ID: 2xzl]. The most shared 1A, 1B, 2A, and 2B/2B-like domains and unstructured C-terminus are colored in blue, brown, cyan, green, and red, respectively. The trans-esterase domain and N terminal domains of *E.coli* TraI, the 2C domain and Pif1-family specific sequence of *S. cerevisiae* Pif1, and the cysteine-histidine-rich CH domain, stalk helices, 1C domain, and the RecA domain of human Upf1ΔCH and *S. cerevisiae* Upf1 are colored in pink, cornflower, forest red, orange red, medium blue, purple, orange, and magenta, respectively. Molecular graphics and analyses were performed with UCSF Chimera, developed by the Resource for Biocomputing, Visualization, and Informatics at the University of California, San Francisco [37].

Table 3 Studies that propose or support the dimer model for wild-type UvrD

Method(s)	Result(s)	References
Single turnover DNA-unwinding experiments (Stopped flow)	A dimer was required to unwind 18-bp dsDNA with a 20-nt 3' ssDNA tail for wild-type UvrD.	[16]
DNA unwinding burst signal analysis (Single-molecule DNA manipulation using magnetic tweezers)	Two wild-type UvrD molecules subsequently bound to the DNA to unwind DNA.	[17]
Quantification of single protein molecules (Fluorescence imaging)	Two or three wild-type UvrD molecules were involved in unwinding 18-bp dsDNA with a 20-nt 3' ssDNA tail.	[18]
Quantification of single UvrD molecules (Fluorescence imaging) DNA-unwinding activity measurement (Single-molecule DNA manipulation using optical tweezers)	Two wild-type UvrD molecules were required for long-distance DNA unwinding.	[19,20]
Conformational change detection of single protein molecules DNA unwinding assay (Single-molecule FRET imaging)	The binding of a second wild-type UvrD monomer altered the conformation of a prebound wild-type UvrD monomer and triggered DNA unwinding.	[21]

to 2 in the DNA unwinding assay [16].

A single-molecule DNA-manipulation study conducted by Sun et al. using magnetic tweezers [17] also supports the dimer model for UvrD (Table 3). They measured DNA unwinding by wild-type UvrD using magnetic tweezers and analyzed the on-time as the duration of an unwinding burst and off-time as the time between two adjacent unwinding burst signals. They concluded that two wild-type UvrD molecules bind to DNA to unwind it because the off-time distributions consisted of two exponential components.

Single-Molecule Direct Visualization of Fluorescently Labeled Wild-Type UvrD

In contrast to conventional biochemical and genetic approaches that provide data on ensemble averages of a large number of molecules, single-molecule fluorescence imaging can observe the behavior of non-averaged individual biomolecules in real time, enabling the unraveling of their dynamics [38].

Yokota et al. applied the single-molecule fluorescence imaging technique to visualize single wild-type UvrD molecules. They first improved the surface coating method with polyethylene glycol (PEG) and succeeded in reducing non-specific protein adsorption on the glass surface to 1/10 that of the conventional method [39]. Next, they simultaneously imaged the association/dissociation of wild-type UvrD molecules with/from 18-base pair (bp) dsDNA with a 20-nucleotide (nt) 3' ssDNA tail and DNA-unwinding dynamics in the presence of ATP, using total-internal reflection fluorescence microscopy (TIRFM). Thus, they were the first to perform single-molecule quantification of the number of helicases interacting with DNA. [18]. They visualized Cy5-labeled wild-type UvrD interacting with Cy3-labeled DNA attached to the PEGylated glass surface via streptavidin–biotin interactions. Since Cy3 was attached to one of the two oligonucleotides that formed the DNA, DNA unwinding completion, where the Cy3-labeled oligonucleotide came off, was monitored through the disappearance of Cy3 fluorescence (Fig. 2A). They observed many traces with a multiple-step (two-step or three-step) increase in Cy5 fluorescence intensity just before completion of the DNA-unwinding process (Fig. 2B and C). The Cy5 fluorescence intensity decreased nearly simultaneously with the Cy3 fluorescence intensity decrease, which showed that the wild-type UvrD dissociated from DNA just after completing DNA unwinding. The traces with multiple steps demonstrated that two or three wild-type UvrD molecules participate in DNA unwinding. Fig. 2D shows the experimentally obtained and theoretically predicted distributions (one-, two-, and three-molecule models) of the number of step changes in the Cy5 fluorescence just before or after DNA unwinding. The ratios of the one-, two-, and three-molecule models were calculated based on the estimated number of Cy5 dye molecules per wild-type UvrD. The experimentally obtained ratios of the step numbers of the Cy5 fluorescence changes agreed better with the two-molecule model than with the one-molecule model. These results thus support the dimer model for UvrD.

Other studies using single-molecule fluorescence imaging, which also support the dimer model for UvrD, were performed using single-molecule force-fluorescence microscopy or single-molecule FRET imaging (Table 3 and Fig. 2E–

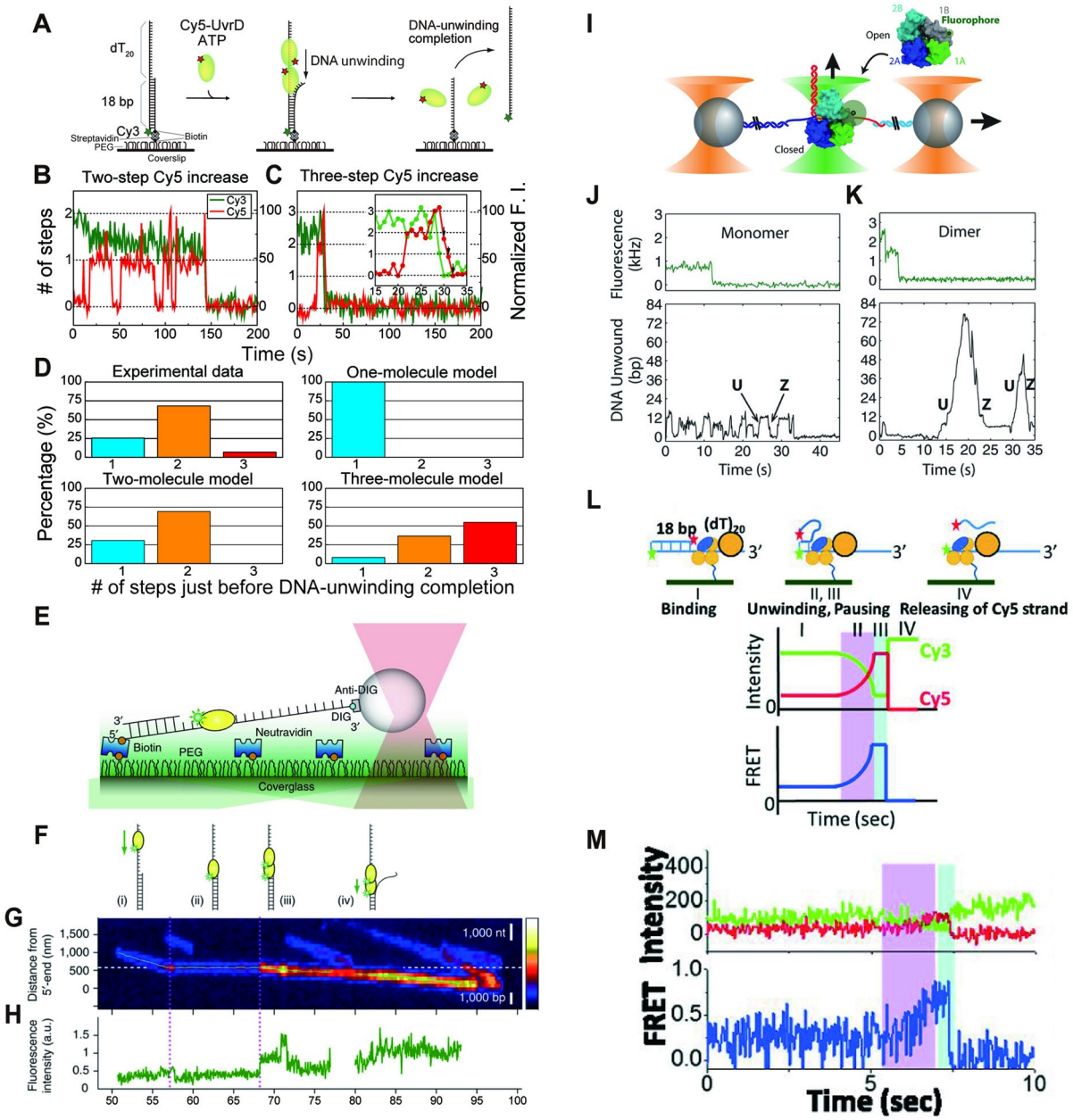

Figure 2 Single-molecule direct visualization studies supporting the dimeric-helicase model for wild-type UvrD. (A–D) Simultaneous single-molecule visualization of DNA unwinding by wild-type UvrD and the association/dissociation events between the helicase and DNA in a solution containing 2 nM Cy5-labeled wild-type UvrD and 1 mM ATP. (A) Schematic representation of the assay. Lasers for exciting Cy3 at 532 nm and Cy5 at 637 nm were incident on the sample plane with objective-type total-internal fluorescence microscopy (TIRFM). Single-molecule fluorescence signals from Cy3-DNA and Cy5-UvrD were simultaneously imaged using a dual-view apparatus. (B, C) Typical time traces of the Cy3- and Cy5-fluorescence intensities (FI), where the Cy5-fluorescence intensity increased in a two-step manner (B) and a three-step manner (indicated with arrows) (C) just before DNA unwinding, resulting in the Cy3 fluorescence disappearance. The three-step fluorescence decrease is indicated with arrows. (D) Experimentally obtained and theoretically predicted distributions (one-molecule, two-molecule, and three-molecule models) of the number of step changes in the Cy5 fluorescence just before or after DNA unwinding. (E–H) Quantification of single UvrD molecules that unwound DNA tethered by single trap optical tweezers. (E) Schematic of the experimental setup for single-molecule force-fluorescence microscopy. Single-molecule fluorescence imaging and single-molecule DNA manipulation were performed by TIRFM and optical tweezers, was attached to a polystyrene bead confined in the optical trap (pink). *(Figure legend continued on next page)*

(F) Schematic drawings of an observed unwinding event: (i) One UvrD molecule is translocated until it encounters an ssDNA/dsDNA junction; (ii) then stops at the junction; (iii) the second UvrD molecule binds to the junction; and (iv) the UvrD dimer unwinds the dsDNA. (G) A kymogram of the unwinding event. (H) The time trace of the fluorescence intensity. (I–K) Quantification of single UvrD molecules that unwind DNA tethered by dual trap optical tweezers. (I) Schematic of the experimental setup for single-molecule force-fluorescence microscopy. Single-molecule fluorescence imaging and single-molecule DNA manipulation were performed by TIRFM and optical tweezers, respectively. Each end of the DNA substrate containing a hairpin was attached to two polystyrene beads confined in the optical trap (orange). (J, K) Representative time traces of unwinding activity and FI for a UvrD monomer (J) and dimer (K), respectively. (Upper panels) Fluorescence from a monomer (A) and a dimer (B) photobleached in one step and two steps, respectively. (Lower panels) Simultaneous measurements of hairpin unwinding (U) and rezipping (Z). The UvrD monomer displays frustrated unwinding, whereas the dimer displays long-distance unwinding. (L, M) Single-molecule FRET imaging of DNA unwinding activation upon second UvrD molecule binding to DNA. (L) Schematic of the expected DNA-unwinding phases. (Phase I) a DNA substrate labeled with Cy3 and Cy5 bound to a UvrD monomer immobilized via streptavidin–biotin interactions on pegylated glass surface, then binding of Cy3/Cy5-DNA to UvrD on the surface. (Phase II colored in magenta) a second UvrD monomer bound to the DNA initiates DNA unwinding which changes Cy3 and Cy5 FIs in an anticorrelated fashion. (Phase III colored in cyan) a temporary plateau in FRET efficiency. (Phase IV) DNA unwinding is completed, and the Cy5-labeled strand diffuses away. (M) A time trace of Cy3 and Cy5 FIs in the presence of 5 μM ATP. (A–D) Reproduced with permission from [18], Copyright © 2013, Biophysical Society. (E–H) Reproduced with permission from [19] with some modifications, available under a Creative Commons License (Attribution-NonCommercial-ShareAlike 3.0 Unported Licence). (I–K) Reproduced with permission from [20], Copyright © 2015, American Association for the Advancement of Science. (L, M) Reproduced with permission from [21] under the PNAS license to publish.

M). Studies using single-molecule force-fluorescence microscopy simultaneously monitored the DNA-unwinding activity of wild-type UvrD with optical tweezers, as well as the number of wild-type UvrD molecules involved in DNA unwinding, by single-molecule fluorescence imaging [19,20]. Studies using single-molecule FRET imaging detected conformational changes in single wild-type UvrD molecules and monitored the DNA unwinding process of single wild-type UvrD molecules [21].

Lee et al. visualized the translocation of single wild-type UvrD molecules onto stretched knt-long ssDNA [19] (Fig. 2E). They found that wild-type UvrD monomer translocation was blocked at the ssDNA/dsDNA junction and that another wild-type UvrD monomer bound to the prebound wild-type UvrD monomer initiated DNA unwinding (Fig 2F). The number of wild-type UvrD monomer(s) was determined from the fluorescence intensity of Cy3 attached to the UvrD monomer(s) (Fig. 2G and H). Comstock et al. visualized efficient DNA unwinding by two wild-type monomers [20]. They used single-molecule force-fluorescence microscopy, in which hairpin DNA was pulled by dual-trap optical tweezers (Fig. 2I). They found that a wild-type UvrD monomer exhibited limited DNA unwinding activity with a low pulling force (Fig. 2J), whereas two wild-type UvrD monomers displayed long-distance unwinding (Fig. 2K). By single-molecule intra-molecular FRET imaging of UvrD monomers, Nguyen et al. showed that the binding of a second wild-type UvrD monomer to the wild-type UvrD monomer, which was prebound to DNA, shifts the 2B conformation of the prebound wild-type UvrD monomer to a more closed state, resulting in the activation of helicase activity [21]. In addition, by single-molecule FRET imaging of DNA unwinding, they also showed that DNA unwinding was soon completed upon binding of a wild-type UvrD monomer to the wild-type UvrD–DNA complex on a glass surface (Fig. 2L and M).

Monomer Model Proposed Using UvrDΔ40C

The opposing monomer model for UvrD was proposed based on X-ray crystallographic structures of monomeric UvrD [8] and from genetic and biochemical assays in which the C-terminal 40 amino acid deletion mutant, UvrDΔ40C, was used. Mechanic et al. [23,40] proposed a monomer model through integration based on the following observations: (i) genetic-complementation assays using a strain lacking the *uvrD* gene showed that UvrDΔ40C complemented the loss of UvrD and was competent to perform both nucleotide-excision repair and methyl-directed mismatch repair in cells; (ii) examination of self-interaction between UvrDΔ40C molecules with a yeast two-hybrid system indicated that UvrDΔ40C was unable to dimerize; (iii) the molecular mass corresponding to dimeric UvrDΔ40C was not detected by sedimentation experiments; (iv) UvrDΔ 40C could be eluted as a single peak that corresponded to a monomer by size-exclusion chromatography; and (v) ssDNA-binding, ssDNA-stimulated ATPase, and DNA-unwinding activities of UvrDΔ40C were almost equivalent to that of wild-type UvrD in vitro. Table 4 summarizes the experimental methods and results of these studies.

Table 4 Studies that propose or support the monomeric-helicase model using UvrDΔ40C

Method	Result(s)	References
X-ray crystallography	Monomeric structures of UvrDΔ40C–DNA complexes were obtained.	[8]
Genetic-complementation assays	UvrDΔ40C was capable of DNA mismatch repair and DNA nucleotide excision repair.	[40]
Yeast two-hybrid screen	No interaction between UvrDΔ40C molecules was detected.	[23]
Sedimentation-equilibrium experiments	All of the data for UvrDΔ40C were most consistent with a model for a single-ideal species with a monomeric molecular mass.	[23]
Velocity-sedimentation experiments	No population of UvrDΔ40C dimers was indicated.	[23]
Size-exclusion chromatography	UvrDΔ40C eluted as a single peak corresponding to a UvrDΔ40C monomer.	[23]
DNA-binding assays	UvrDΔ40C had comparable 90-nt ssDNA binding affinity to wild-type UvrD. K_D = 276 ± 18 nM (wild-type) and K_D = 345 ± 16 nM (Δ40C) in the absence of nucleotide K_D = 11 ± 1 nM (wild-type) and K_D = 24 ± 13 nM (Δ40C) in the presence of 1 mM AMP-PNP	[40]
DNA-stimulated ATP hydrolysis	UvrDΔ40C showed similar ATPase activity to wild-type UvrD. k_{cat} = 147 ± 21 s^{-1} (wild-type) and k_{cat} = 157 ± 14 s^{-1} (Δ40C) K_m = 62 ± 11 μM (wild-type) and K_m = 50 ± 9 μM (wild-type)	[40]
DNA-unwinding assays	UvrDΔ40C exhibited the equivalent DNA unwinding activity to wild-type UvrD.	[40]
	The rate of DNA unwinding by UvrDΔ40C was slightly greater than that of wild-type UvrD.	[23]

C-Terminal-Truncated UvrD

UvrDΔ40C lacks 40 amino acids in the C-terminal region but all helicase motifs in the four structural domains are intact. Many studies have indicated that the C-terminus plays essential roles in nucleic acid binding for many proteins with helicase and dimerization activities, and the role of the C-terminus has been well studied for SF2 DEAD-box helicases [41].

Several studies have reported the effect of longer C-terminal amino acid deletion on the function of UvrD (UvrDΔ73C, UvrDΔ102C, or UvrDΔ107C) [35,40]. UvrDΔ102C and UvrDΔ107C were unable to mediate DNA repair in vivo. UvrDΔ73C showed a slightly reduced ssDNA-binding affinity, whereas UvrDΔ102C exhibited a reduced ssDNA-binding affinity. The ssDNA-binding activity coincided with the ATPase and DNA-unwinding characteristics; thus, UvrDΔ73C retained ATPase and DNA-unwinding abilities, whereas UvrDΔ102C lost these abilities. The UvrDΔ102C mutant lacked both the unstructured C-terminus and a part of the conserved 2A domain, thus revealing that the 2A domain is crucial for UvrD function. In addition, the length of the remaining unstructured C-terminal region is probably related to the DNA unwinding activity. Maluf et al. suggested that UvrDΔ40C is possibly dimerized, as they provided data that UvrDΔ73C could dimerize, which was obtained by analytical-sedimentation–equilibrium-ultracentrifugation experiments [42]. However, the dimerization equilibrium constant was 25 times lower than that of wild-type UvrD. Table 5 summarizes the effects of deleting C-terminal amino acids from UvrD on its function and oligomerization state.

Table 5 Effects of deleting C-terminal amino acids from UvrD on its functions and oligomerization state

UvrD	DNA repair	DNA-stimulated ATPase	DNA binding	DNA unwinding	Oligomerization state in vitro	Oligomerization state in vivo	References
UvrDΔ40C	+ [1)]	+	+	+	Monomer	Monomer	[23,40]
UvrDΔ73C	+ [2)]	+	+	+	Dimer	N.D.	[35,42]
UvrDΔ102C	− [1)]	−	−	−	N.D.	N.D.	[40]
UvrDΔ107C	− [1)]	N.D.	N.D.	N.D.	N.D.	N.D.	[40]

[1)] Experiments were performed in vivo. [2)] Experiments were performed in vitro. +: Activity was detected. -: Activity was not detected. N.D.: Not determined.

Single-Molecule Direct Visualization of Fluorescently Labeled UvrDΔ40C

Since the monomer model for UvrD was proposed using UvrDΔ40C, single-molecule direct visualization of fluorescently labeled UvrDΔ40C was performed [22] to address the question of whether multiple UvrDΔ40C molecules are involved in DNA unwinding, similar to wild-type UvrD.

An 18-bp dsDNA with a 20-nt 3' ssDNA tail, the same DNA substrate used in the single-molecule direct visualization of wild-type UvrD, was used and immobilized on the PEGylated glass surface via streptavidin–biotin interactions. One of the two oligonucleotides was labeled with biotin for glass surface immobilization, and the other was labeled with Cy3. The completion of DNA unwinding was detected by the disappearance of Cy3 fluorescence (Fig. 3A). Then, Buffer U solution (6 mM NaCl, 2.5 mM $MgCl_2$, 10% glycerol, and 25 mM Tris-HCl (pH 7.5)), containing Cy5-labeled UvrDΔ40C and ATP, was infused into the flow cell.

As observed for wild-type UvrD, the Cy3 and Cy5 fluorescence intensities decreased almost simultaneously after the Cy5 fluorescence intensity increased in two steps, suggesting that DNA unwinding was completed immediately after the binding of the second UvrDΔ40C molecule to the DNA (Fig. 3B). Fig. 3C shows a trace with a three-step Cy5 fluorescence decrease (indicated with arrows), suggesting that three UvrDΔ40C molecules are involved in DNA unwinding. Fig. 3D shows the experimentally obtained distribution and theoretical distributions (one-, two-, and three-molecule DNA unwinding models) of the number of step changes in the Cy5 fluorescence intensity just before or after DNA unwinding. The theoretical distributions were calculated based on the labeling rate of Cy5-UvrDΔ40C (79%) and dwell time for the second UvrDΔ40C association. The distribution of the one- and two-step fluorescence changes in the experimentally obtained traces was closest to that of the two-molecule model. Fitting the experimentally obtained distribution with a linear combination of the predicted models was used to estimate the percentages of the one-, two-, and three-molecule models, which were 1%, 92%, and 7%, respectively. Therefore, these results indicate that not a single UvrDΔ40C molecule but two or three UvrDΔ40C molecules are mostly involved in unwinding DNA.

Association/Dissociation Dynamics for the UvrDΔ40C–DNA Interaction

UvrDΔ40C association/dissociation events were then analyzed based on the kinetic scheme of the UvrD–DNA interaction [22] (Fig. 4A). The stepwise Cy5-fluorescence increases or decreases were interpreted as UvrDΔ40C association or dissociation events, respectively. Fig. 4B shows the dwell-time distribution of the indicated states involving up to two UvrDΔ40C molecules (excluding the dwell time just before completion of the DNA-unwinding process). The mean association/dissociation rate constants were obtained by fitting the distributions using a single exponential. A comparison of the obtained association and dissociation rate constants with those of the wild-type UvrD showed that the association and dissociation rate constants of the first UvrD molecule (k_1, k_{-1}) were comparable, whereas those of the second UvrD molecule (k_2, k_2) were approximately 2.5 fold higher for UvrDΔ40C (Fig. 4C). This result indicated that the deletion of the C-terminal amino acid affects the DNA association and dissociation of the second bound UvrD molecule

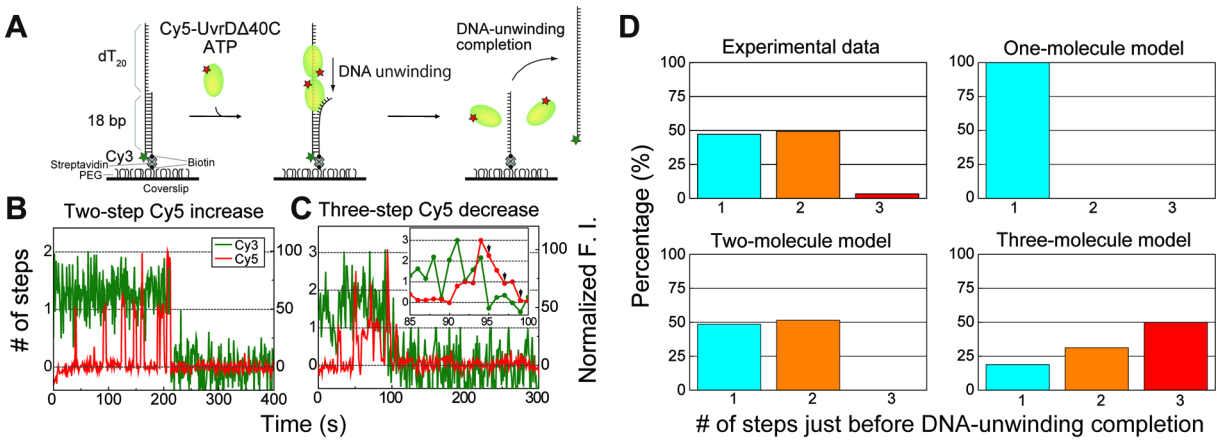

Figure 3 Simultaneous single-molecule visualization of DNA unwinding by UvrDΔ40C and the association/dissociation events between the helicase and DNA in a solution containing 2 nM Cy5-UvrDΔ40C and 1 mM ATP. (A) Schematic representation of the assay. (B, C) Typical time traces of the Cy3- and Cy5- FI, where the Cy5-FI increased in a two-step manner (B) and decreased a three-step manner (indicated with arrows) (C) just before DNA unwinding, resulting in the Cy3 fluorescence disappearance. (D) Experimentally obtained and theoretically predicted distributions (one-molecule, two-molecule, and three-molecule models) of the number of step changes in the Cy5 fluorescence, just before or after DNA unwinding. Reproduced with permission from [22], Copyright © 2020, Biophysical Society.

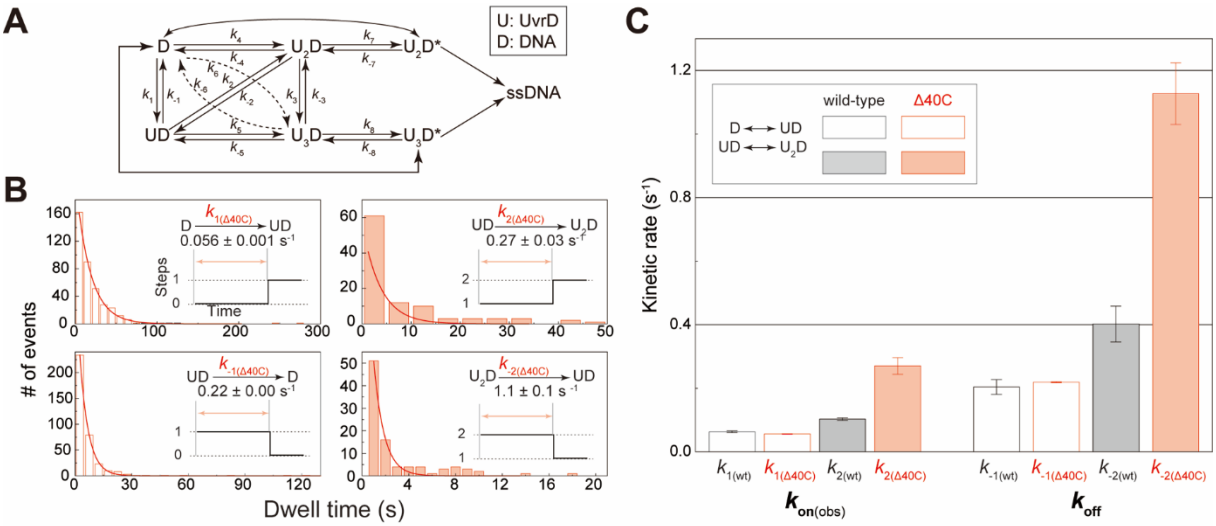

Figure 4 Association- and dissociation-rate constants for UvrDΔ40C–DNA interaction. (A) Kinetic scheme of the UvrD–DNA interaction. U and D represent UvrD and DNA, respectively. (B) Dwell-time distributions of the indicated states. Association- and dissociation-rate constants were obtained by a single exponential fit of each distribution. $K_{on(obs)}$ are association rate constants under 2 nM UvrDΔ40C concentration. (C) Comparison of the obtained rate constants between UvrDΔ40C and wild-type UvrD. $K_{on(obs)}$ are the observed association rate constants under 2 nM UvrDΔ40C concentration. The error bars represent the standard errors. Reproduced with permission from [22], Copyright © 2020, Biophysical Society.

rather than the first bound UvrD molecule, which suggests that UvrDΔ40C molecules form a dimer less frequently than wild-type UvrD.

Multiple UvrDΔ40C Molecules Are Likely to Form an Oligomer to Unwind DNA

The two or three UvrDΔ40C molecules that bound to DNA just before completion of the DNA-unwinding process presumably interacted with each other and formed an oligomer on the ssDNA tail. The self-interaction and oligomer formation on DNA were originally proposed from a non-linear sigmoidal dependence of DNA unwinding efficiency on [wild-type UvrD]/[DNA] [16], which cannot be explained by the "independent monomer" model. The independent monomer model has been proposed for some helicases, such as Dda [31] and RecQ [43], which states that these helicases can unwind DNA without self-interaction or oligomerization.

To test this self-interaction hypothesis, a single-molecule DNA-unwinding assay was performed using a dsDNA substrate with a shorter 3' ssDNA tail (18-bp DNA with a 12-nt 3' ssDNA tail) [22] (Fig. 5A). The assay demonstrated that two or three UvrDΔ40C molecules are bound just before completion of the DNA-unwinding process (Fig. 5B and C), even though the DNA had a minimum ssDNA overhang length (12 nt) required to unwind 18-bp dsDNA. This result, together with the reported results that (1) wild-type UvrD molecules are difficult to bind to blunt dsDNA [18] and (2) each wild-type UvrD molecule supposedly occupies ssDNA length of 10 ± 2 nt [44], suggests that multiple UvrDΔ40C molecules are present on DNA during DNA unwinding. These results support the self-interaction or oligomerization of UvrDΔ40C molecules on DNA, which is further supported by single-molecule FRET imaging. The observed conformational change in the 2B domain and DNA unwinding activation (Fig. 2L and M) induced by binding of a second wild-type UvrD monomer indicated some physical contact between UvrD molecules on ssDNA.

Possible Reasons for the Discrepancy between the Conclusions Obtained by the Single-Molecule Direct Visualization Study and the Studies That Proposed the Monomer Model

The preceding sections described the results obtained by single-molecule direct visualization study that not only wild-type UvrD but also UvrDΔ40C unwound DNA presumably in an oligomeric form, which contradicts the conclusion obtained by biochemical and genetic studies that UvrDΔ40C unwinds DNA in a monomeric form. This section discusses possible reasons for this discrepancy. Table 6 lists the buffer conditions and DNA substrates used in the single-molecule direct visualization and studies using genetic and biochemical assays on UvrDΔ40C.

A first plausible reason for this discrepancy may be the difference in the DNA substrates used. Mechanic et al. performed velocity sedimentation and size-exclusion chromatography in the absence and presence of 16-nt ssDNA, and concluded

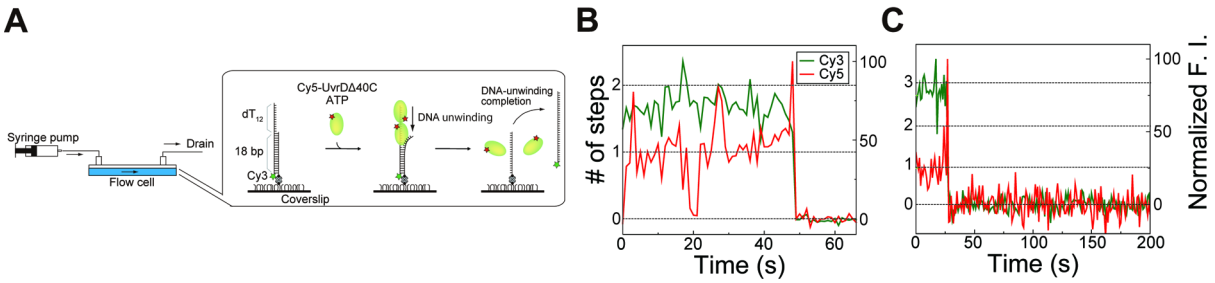

Figure 5 Simultaneous single-molecule visualization of DNA unwinding by UvrDΔ40C and the association/dissociation events between the helicase and DNA substrate with a 12-nt 3′ ssDNA tail in a solution containing 10 nM Cy5-UvrDΔ40C and 1 mM ATP. (A) Schematic representation of the assay. (B) Time traces of the Cy3- and Cy5-FIs, where the Cy5-FI increased in a two-step manner just before DNA unwinding, resulting in the Cy3 fluorescence disappearance; (C) time traces of the Cy3- and Cy5-FIs, where the maximum Cy5-FI was supposed to come from three Cy5-UvrDΔ40C molecules just before the DNA unwinding process. Reproduced with permission from [22], Copyright © 2020, Biophysical Society.

that UvrDΔ40C was monomeric regardless of the presence or absence of DNA. They did not detect the dimeric UvrDΔ40C probably because they did not use a dsDNA substrate with an ssDNA/dsDNA junction and 3′ ssDNA tail. Maluf et al. [16] and Yokota et al. [18] showed that wild-type UvrD has a high affinity for the ssDNA/dsDNA junction. Therefore, Mechanic et al. possibly failed to detect binding of multiple UvrDΔ40C molecules to ssDNA.

A second reason for this discrepancy may be the difference in buffer compositions. Mechanic et al. used buffers containing 20 mM NaCl to examine and compare the biochemical characteristics of UvrDΔ40C with those of wild-type

Table 6 Buffer conditions and DNA substrates used in the single-molecule direct visualization and studies using genetic and biochemical assays on UvrDΔ40C

	Method	NaCl (mM)	$MgCl_2$ (mM)	Glycerol (%)	pH	2-ME (mM)	Temperature (ºC)	DNA substrate(s)
Yokota, Biophys. J. 2020 [22]	DNA-unwinding assays (Low salt)	6	2.5	10	7.5	0	25	18-bp 3′-$(dT)_{20}$ 18-bp 3′-$(dT)_{12}$
	DNA-unwinding assays (High salt)	200	3	10	7.5	5	25	18-bp 3′-$(dT)_{20}$
Mechanic et al., J. Bacteriol. 1999 [40]	DNA-binding assays	20	3	10	7.5	5	37	90-nt ssDNA
	ATPase assays	20	3	0	7.5	5	37	7.2-knt ssDNA
	DNA-unwinding assays	20	3	0	7.5	5	25	238-bp blunt dsDNA
Mechanic et al., J. Biol. Chem. 1999 [23]	Sedimentation-equilibrium experiments	200	3	20	8.3	15	25	Not used
	Velocity-sedimentation experiments	50	3	20	7.5	5	25	16-nt ssDNA
	Size-exclusion chromatography experiments	100	3	20	7.5	5	4	16-nt ssDNA
	DNA-unwinding assays	20	3	0	7.5	5	37	92-bp partial dsDNA 7.2-knt ssDNA

2-ME: 2-mercaptoethanol. 18-bp 3′-$(dT)_{20}$: 18-bp dsDNA with a 20-nt 3' ssDNA tail. 18-bp 3′-$(dT)_{12}$: 18-bp dsDNA with a 12-nt 3' ssDNA tail.

UvrD [23,40]. The authors reported that UvrDΔ40C had ssDNA-binding, ssDNA-stimulated ATPase, and dsDNA-unwinding activities comparable to those of wild-type UvrD. However, the conditions of these experiments were quite different (20 mM NaCl, 0 or 10% glycerol) from those used for analytical-sedimentation-equilibrium ultracentrifugation and size-exclusion chromatography experiments (100 or 200 mM NaCl, 20% glycerol), which concluded that UvrDΔ40C was active as a monomer. Maluf et al. reported that UvrDΔ40C may form a dimer while unwinding DNA, and the above experiments by Mechanic et al. were performed in a solution with a low NaCl concentration (20 mM), in the absence of glycerol, at a low pH (7.5), and at a high temperature (37°C), which were favorable for oligomer formation. The authors detected the association of multiple UvrDΔ40C molecules with DNA in Buffer U (6 mM NaCl, 10% glycerol).

A third possible explanation for the discrepancy may be the shorter temporal interaction of the second UvrDΔ40C for DNA than wild-type UvrD. As described previously, the dissociation rate for the second UvrDΔ40C monomer was estimated to be approximately 2.5-fold larger than that for wild-type UvrD, indicating that the binding of the second UvrDΔ40C monomer to DNA is transient. This makes the detection of the binding of multiple UvrDΔ40C molecules more difficult.

Implications of Unwinding Activity of UvrD In Vivo

In the previous section, the use of high- and low-NaCl solutions has been discussed. In addition, Buffer U used in the single-molecule visualization study contained a low NaCl concentration of 6 mM, which was significantly lower than physiological conditions and unlike the buffer conditions used for biochemical analyses by Mechanic et al. [23]. Thus, another single-molecule visualization was performed under a physiologically relevant buffer condition with a higher NaCl concentration (200 mM NaCl) (Fig. 6A). This buffer condition was analogous to that used in the velocity-ultracentrifugation experiments by Mechanic et al. [23] and was reported to be more unfavorable for dimer formation. The visualization showed a two-step increase in Cy5 fluorescence (Fig. 6B) as well as Cy5 fluorescence increases with a two or more fold increase in intensity compared to those of the Cy5-fluorescence intensity increases from one Cy5-UvrDΔ40C (Fig 6C), just before completion of the DNA-unwinding process. These results indicate that two UvrDΔ40C molecules can bind to the DNA and that multiple UvrDΔ40C molecules are also involved in DNA unwinding even under high-salt physiologically-relevant salt conditions.

Visualization under physiologically relevant salt conditions also showed that the association rate for UvrDΔ40C under high-salt conditions was much lower than that under 6 mM NaCl. It was reported that the UvrD concentration in vivo was 1.4–4 μM (1,000–3,000 molecules/cell) [45] and that the effective concentration of a nick in the genomic DNA in vivo, which is created by other DNA repair enzymes near a damaged or mismatch DNA, was ~1 nM. The UvrD and nick concentrations were much higher (several thousand and several hundred times, respectively) than those used for the single-molecule assays (UvrDΔ40C and ssDNA/dsDNA junction concentrations were 2 nM and 10 nM or ~3 pM, respectively). Thus, UvrDΔ40C association events must occur much more frequently in vivo than in single-molecule visualization. Finally, the association of multiple UvrDΔ40C molecules with DNA and their participation in DNA unwinding observed under the 200 mM NaCl condition is relevant to UvrD function in vivo, although the *in vivo* environment, including high crowding conditions, would somehow modulate the dimerization of UvrD on DNA.

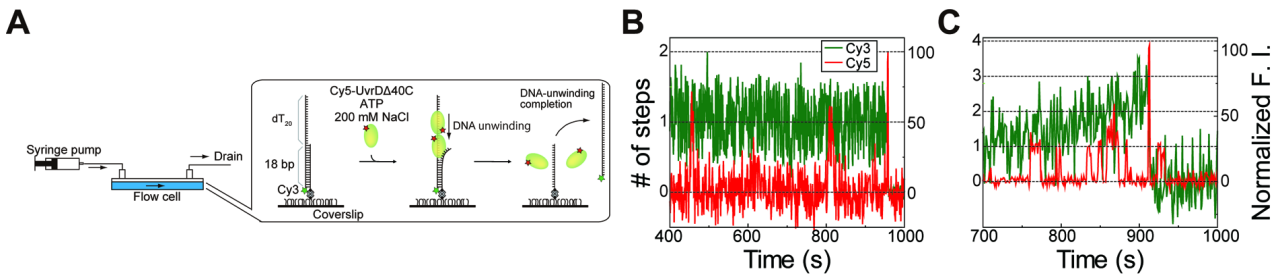

Figure 6 Simultaneous single-molecule visualization of DNA unwinding driven by Cy5-UvrDΔ40C and the association/dissociation events between the helicase and DNA in the presence of 1 mM ATP and 200 mM NaCl in solution. (A) Schematic representation of the assay. (B) Time traces of the Cy3- and Cy5-FIs, where the Cy5-FI increased by approximately two-fold just before DNA unwinding compared to those observed for two single-step Cy5-FI increases, and the Cy3-FI decreased to its background level (Cy5-UvrDΔ40C concentration = 2 nM). (C) Time traces of the Cy3- and Cy5-FIs, where the Cy5-FI increased by more than two-fold just before the DNA unwinding process compared to those observed for single-step Cy5-FI increases (Cy5-UvrDΔ40C concentration = 10 nM). Reproduced with permission from [22], Copyright © 2020, Biophysical Society.

Summary and Perspectives

This paper provides a brief explanation of the classification of helicase SFs based on structural homology and introduces two opposing non-hexameric helicase models concerning SF1 helicases. This paper reviews past and recent studies on UvrD, including the single-molecule direct visualization of wild-type UvrD and a UvrD mutant lacking the C-terminal 40 amino acids (UvrDΔ40C), the latter of which was used in genetic and biochemical assays supporting a monomer model. The visualization revealed that multiple UvrDΔ40C molecules jointly unwound DNA, which is more likely in an oligomeric form.

Generally speaking, rarely occurring and transient protein–DNA interactions are difficult to detect by conventional biochemical ensemble measurements, because the interaction is frequently buried in static and averaged data. In contrast, as reviewed in this paper, direct visualization of single protein molecules is of great utility and is capable of detecting such interactions without ensemble averaging in real time.

The reason why dimeric UvrD is necessary for efficient DNA unwinding has not yet been fully elucidated. If X-ray crystallographic structures of dimeric UvrD were available, they could provide deep insights into this fundamental question. However, since previous research regarding them is lacking, this is unfeasible at present. Meanwhile, a single-molecule FRET imaging study provided an important clue to resolve this question, indicating that an intra-molecular conformational change of monomeric UvrD induced by dimer formation increases helicase activity. The imaging study showed that the interaction of a late-coming UvrD monomer with a UvrD monomer prebound to DNA shifts the 2B domain conformation of the prebound UvrD monomer, causing activation of helicase activity and triggering the completion of DNA unwinding (Fig. 2L and M). The 2B domain movement of UvrD was also observed using single-molecule force-fluorescence microscopy [20]. The catalytic role of the 2B domain in DNA unwinding was originally proposed based on the crystal structures of SF1 helicases, including UvrD, PcrA, and Rep [8,11,46]. Intriguingly, conformational fixation of the 2B domain of PcrA and Rep by intramolecular crosslinking dramatically increases its unwinding processivity (>1000 bp) [47,48].

A recently published paper reported on the direct measurement of UvrD stepping dynamics (unwinding and re-zipping DNA) under various ATP concentrations using high-resolution optical tweezers [49]. The stepping mechanism modeled based on single-molecule measurements and molecular dynamics (MD) simulations is consistent with the notion that UvrD unwinds 1 bp per ATP hydrolysis cycle. The step size, which is defined as the average number of bp unwound between successive rate-limiting steps, was estimated for monomeric and dimeric UvrD. The estimated average step sizes were nearly the same (~3 bp), indicating that dimerization did not significantly affect the unwinding step size. Thus, detailed coupling between ATP hydrolysis and DNA unwinding, that is, how the energy derived from ATP hydrolysis is utilized by each monomeric UvrD consisting of a UvrD dimer, remains unknown and merits further study.

Past structural and biophysical studies have shown that protein oligomerization is a critical factor in the regulation of many proteins [50], such as enzymes, ion channels, receptors, and transcription factors. Oligomerization plays an essential role in the regulation of protein activity and structural stability. It has been reported that more than 35% of intracellular proteins exist in an oligomeric state, including dimers [51]. The Brenda enzyme database (https://www.brenda-enzymes.org/), the most comprehensive enzyme repository, lists only about one-fourth of enzymes as monomers.

Direct single-molecule observation of UvrD will further elucidate the interrelation among the C-terminal amino acids and oligomer formation, DNA unwinding activity, and ATPase activity, which can be applied to other helicases. This interrelation should be investigated using a more severe form of deletion mutants. Yokota recently performed single-molecule direct visualization of UvrDΔ73C and obtained preliminary results indicating that two UvrDΔ73C molecules are also involved in DNA unwinding, presumably in an oligomeric form. Therefore, single-molecule direct visualization of nucleic acid-binding proteins provides quantitative and kinetic information to reveal their fundamental mechanisms. Furthermore, the visualization can help identify transient and minor populations that are usually overlooked by conventional ensemble averaging-based measurements and determine kinetic rate constants, which will enlarge our understanding of protein–nucleic acid interactions.

Conflict of Interest

The author declares that there are no conflicts of interest.

Author Contributions

H.Y. wrote the manuscript.

Acknowledgements

This work was supported by the Japan Society for the Promotion of Science (JSPS) Grants-in-Aid for Scientific Research (KAKENHI) under grant numbers JP15H01648, JP17H05892, JP18K06169, and JP21K06103.

References

[1] Friedberg, E. C., Walker, G. C., Siede, W., Wood, R. D. DNA Repair and Mutagenesis: Second edition (ASM Press, Washington D.C., 2005).
[2] Yokota, H. DNA unwinding and oligomerization dynamics of *Escherichia coli* UvrD helicase revealed by single-molecule fluorescence imaging. SEIBUTSU BUTSURI 61, 227–231 (2021). https://doi.org/10.2142/biophys.61.227
[3] Singleton, M. R., Dillingham, M. S., Wigley, D. B. Structure and mechanism of helicases and nucleic acid translocases. Annu. Rev. Biochem. 76, 23–50 (2007). https://doi.org/10.1146/annurev.biochem.76.052305.115300
[4] Singleton, M. R., Sawaya, M. R., Ellenberger, T., Wigley, D. B. Crystal structure of T7 gene 4 ring helicase indicates a mechanism for sequential hydrolysis of nucleotides. Cell 101, 589–600 (2000). https://doi.org/10.1016/S0092-8674(00)80871-5
[5] Enemark, E. J., Joshua-Tor, L. On helicases and other motor proteins. Curr. Opin. Struct. Biol. 18, 243–257 (2008). https://doi.org/10.1016/j.sbi.2008.01.007
[6] Fairman-Williams, M. E., Guenther, U. P., Jankowsky, E. SF1 and SF2 helicases: Family matters. Curr. Opin. Struct. Biol. 20, 313–324 (2010). https://doi.org/10.1016/j.sbi.2010.03.011
[7] Gilhooly, N. S., Gwynn, E. J., Dillingham, M. S. Superfamily 1 helicases. Front. Biosci. (Schol. Ed.) 5, 206–216 (2013). https://doi.org/10.2741/S367
[8] Lee, J. Y., Yang, W. UvrD helicase unwinds DNA one base pair at a time by a two-part power stroke. Cell 127, 1349–1360 (2006). https://doi.org/10.1016/j.cell.2006.10.049
[9] Jia, H., Korolev, S., Niedziela-Majka, A., Maluf, N. K., Gauss, G. H., Myong, S., et al. Rotations of the 2B sub-domain of *E. coli* UvrD helicase/translocase coupled to nucleotide and DNA binding. J. Mol. Biol. 411, 633–648 (2011). https://doi.org/10.1016/j.jmb.2011.06.019
[10] Korolev, S., Hsieh, J., Gauss, G. H., Lohman, T. M., Waksman, G. Major domain swiveling revealed by the crystal structures of complexes of *E. coli* Rep helicase bound to single-stranded DNA and ADP. Cell 90, 635–647 (1997). https://doi.org/10.1016/s0092-8674(00)80525-5
[11] Velankar, S. S., Soultanas, P., Dillingham, M. S., Subramanya, H. S., Wigley, D. B. Crystal structures of complexes of PcrA DNA helicase with a DNA substrate indicate an inchworm mechanism. Cell 97, 75–84 (1999). https://doi.org/10.1016/s0092-8674(00)80716-3
[12] Ilangovan, A., Kay, C. W. M., Roier, S., El Mkami, H., Salvadori, E., Zechner, E. L., et al. Cryo-EM structure of a relaxase reveals the molecular basis of DNA unwinding during bacterial conjugation. Cell 169, 708–721 (2017). https://doi.org/10.1016/j.cell.2017.04.010
[13] Lu, K. Y., Chen, W. F., Rety, S., Liu, N. N., Wu, W. Q., Dai, Y. X., et al. Insights into the structural and mechanistic basis of multifunctional *S. cerevisiae* Pif1p helicase. Nucleic Acids Res. 46, 1486–1500 (2018). https://doi.org/10.1093/nar/gkx1217
[14] He, X., Byrd, A. K., Yun, M. K., Pemble, C. W., Harrison, D., Yeruva, L., et al. The T4 phage SF1B helicase Dda is structurally optimized to perform DNA strand separation. Structure 20, 1189–1200 (2012). https://doi.org/10.1016/j.str.2012.04.013
[15] Chakrabarti, S., Jayachandran, U., Bonneau, F., Fiorini, F., Basquin, C., Domcke, S., et al. Molecular mechanisms for the RNA-dependent ATPase activity of Upf1 and its regulation by Upf2. Mol. Cell 41, 693–703 (2011). https://doi.org/10.1016/j.molcel.2011.02.010
[16] Maluf, N. K., Fischer, C. J., Lohman, T. M. A dimer of *Escherichia coli* UvrD is the active form of the helicase in vitro. J. Mol. Biol. 325, 913–935 (2003). https://doi.org/10.1016/s0022-2836(02)01277-9
[17] Sun, B., Wei, K. J., Zhang, B., Zhang, X. H., Dou, S. X., Li, M., et al. Impediment of *E. coli* UvrD by DNA-destabilizing force reveals a strained-inchworm mechanism of DNA unwinding. EMBO J. 27, 3279–3287 (2008). https://doi.org/10.1038/emboj.2008.240
[18] Yokota, H., Chujo, Y. A., Harada, Y. Single-molecule imaging of the oligomer formation of the nonhexameric *Escherichia coli* UvrD helicase. Biophys. J. 104, 924–933 (2013). https://doi.org/10.1016/j.bpj.2013.01.014
[19] Lee, K. S., Balci, H., Jia, H., Lohman, T. M., Ha, T. Direct imaging of single UvrD helicase dynamics on long single-stranded DNA. Nat. Commun. 4, 1878 (2013). https://doi.org/10.1038/ncomms2882

[20] Comstock, M. J., Whitley, K. D., Jia, H., Sokoloski, J., Lohman, T. M., Ha, T., et al. Direct observation of structure-function relationship in a nucleic acid-processing enzyme. Science 348, 352–354 (2015). https://doi.org/10.1126/science.aaa0130
[21] Nguyen, B., Ordabayev, Y., Sokoloski, J. E., Weiland, E., Lohman, T. M. Large domain movements upon UvrD dimerization and helicase activation. Proc. Natl. Acad. Sci. U.S.A. 114, 12178–12183 (2017). https://doi.org/10.1073/pnas.1712882114
[22] Yokota, H. DNA-unwinding dynamics of *Escherichia coli* UvrD lacking the C-terminal 40 amino acids. Biophys. J. 118, 1634–1648 (2020). https://doi.org/10.1016/j.bpj.2020.02.014
[23] Mechanic, L. E., Hall, M. C., Matson, S. W. *Escherichia coli* DNA helicase II is active as a monomer. J. Biol. Chem. 274, 12488–12498 (1999). https://doi.org/10.1074/jbc.274.18.12488
[24] Wong, I., Lohman, T. M. Allosteric effects of nucleotide cofactors on *Escherichia coli* Rep helicase-DNA binding. Science 256, 350–355 (1992). https://doi.org/10.1126/science.256.5055.350
[25] Cheng, W., Hsieh, J., Brendza, K. M., Lohman, T. M. *E. coli* Rep oligomers are required to initiate DNA unwinding in vitro. J. Mol. Biol. 310, 327–350 (2001). https://doi.org/10.1006/jmbi.2001.4758
[26] Yang, Y., Dou, S. X., Ren, H., Wang, P. Y., Zhang, X. D., Qian, M., et al. Evidence for a functional dimeric form of the PcrA helicase in DNA unwinding. Nucleic Acids Res. 36, 1976–1989 (2008). https://doi.org/10.1093/nar/gkm1174
[27] Chisty, L. T., Toseland, C. P., Fili, N., Mashanov, G. I., Dillingham, M. S., Molloy, J. E., et al. Monomeric PcrA helicase processively unwinds plasmid lengths of DNA in the presence of the initiator protein RepD. Nucleic Acids Res. 41, 5010–5023 (2013). https://doi.org/10.1093/nar/gkt194
[28] Sikora, B., Eoff, R. L., Matson, S. W., Raney, K. D. DNA unwinding by *Escherichia coli* DNA helicase I (TraI) provides evidence for a processive monomeric molecular motor. J. Biol. Chem. 281, 36110–36116 (2006). https://doi.org/10.1074/jbc.M604412200
[29] Singh, S. P., Koc, K. N., Stodola, J. L., Galletto, R. A monomer of Pif1 unwinds double-stranded DNA and it is regulated by the nature of the non-translocating strand at the 3'-End. J. Mol. Biol. 428, 1053–1067 (2016). https://doi.org/10.1016/j.jmb.2016.02.017
[30] Nanduri, B., Byrd, A. K., Eoff, R. L., Tackett, A. J., Raney, K. D. Pre-steady-state DNA unwinding by bacteriophage T4 Dda helicase reveals a monomeric molecular motor. Proc. Natl. Acad. Sci. U.S.A. 99, 14722–14727 (2002). https://doi.org/10.1073/pnas.232401899
[31] Eoff, R. L., Raney, K. D. Kinetic mechanism for DNA unwinding by multiple molecules of Dda helicase aligned on DNA. Biochemistry 49, 4543–4553 (2010). https://doi.org/10.1021/bi100061v
[32] Bhattacharya, A., Czaplinski, K., Trifillis, P., He, F., Jacobson, A., Peltz, S. W. Characterization of the biochemical properties of the human Upf1 gene product that is involved in nonsense-mediated mRNA decay. RNA 6, 1226–1235 (2000). https://doi.org/10.1017/s1355838200000546
[33] Fiorini, F., Bagchi, D., Le Hir, H., Croquette, V. Human Upf1 is a highly processive RNA helicase and translocase with RNP remodelling activities. Nat. Commun. 6, 7581 (2015). https://doi.org/10.1038/ncomms8581
[34] Kanaan, J., Raj, S., Decourty, L., Saveanu, C., Croquette, V., Le Hir, H. UPF1-like helicase grip on nucleic acids dictates processivity. Nat. Commun. 9, 3752 (2018). https://doi.org/10.1038/s41467-018-06313-y
[35] Manelyte, L., Guy, C. P., Smith, R. M., Dillingham, M. S., McGlynn, P., Savery, N. J. The unstructured C-terminal extension of UvrD interacts with UvrB, but is dispensable for nucleotide excision repair. DNA Repair (Amst) 8, 1300–1310 (2009). https://doi.org/10.1016/j.dnarep.2009.08.005
[36] Lohman, T. M., Bjornson, K. P. Mechanisms of helicase-catalyzed DNA unwinding. Annu. Rev. Biochem. 65, 169–214 (1996). https://doi.org/10.1146/annurev.bi.65.070196.001125
[37] Pettersen, E. F., Goddard, T. D., Huang, C. C., Couch, G. S., Greenblatt, D. M., Meng, E. C., et al. UCSF Chimera-A visualization system for exploratory research and analysis. J. Comput. Chem. 25, 1605–1612 (2004). https://doi.org/10.1002/jcc.20084
[38] Yokota, H. Fluorescence microscopy for visualizing single-molecule protein dynamics. Biochim. Biophys. Acta Gen. Subj. 1864, 129362 (2020). https://doi.org/10.1016/j.bbagen.2019.05.005
[39] Yokota, H., Han, Y. W., Allemand, J.-F., Xi, X. G., Bensimon, D., Croquette, V., et al. Single-molecule visualization of binding modes of helicase to DNA on PEGylated surfaces. Chem. Lett. 38, 308–309 (2009). https://doi.org/10.1246/cl.2009.308
[40] Mechanic, L. E., Latta, M. E., Matson, S. W. A region near the C-terminal end of *Escherichia coli* DNA helicase II is required for single-stranded DNA binding. J. Bacteriol. 181, 2519–2526 (1999). https://doi.org/10.1128/JB.181.8.2519-2526.1999
[41] Yokota, H. Roles of the C-terminal amino acids of non-hexameric helicases: Insights from *Escherichia coli* UvrD. Int. J. Mol. Sci. 22, 1018 (2021). https://doi.org/10.3390/ijms22031018
[42] Maluf, N. K., Lohman, T. M. Self-association equilibria of *Escherichia coli* UvrD helicase studied by analytical

ultracentrifugation. J. Mol. Biol. 325, 889–912 (2003). https://doi.org/10.1016/s0022-2836(02)01276-7
[43] Rad, B., Forget, A. L., Baskin, R. J., Kowalczykowski, S. C. Single-molecule visualization of RecQ helicase reveals DNA melting, nucleation, and assembly are required for processive DNA unwinding. Proc. Natl. Acad. Sci. U.S.A. 112, E6852–E6861 (2015). https://doi.org/10.1073/pnas.1518028112
[44] Runyon, G. T., Wong, I., Lohman, T. M. Overexpression, purification, DNA binding, and dimerization of the *Escherichia coli uvrD* gene product (helicase II). Biochemistry 32, 602–612 (1993). https://doi.org/10.1021/bi00053a028
[45] George, J. W., Brosh, R. M., Jr., Matson, S. W. A dominant negative allele of the *Escherichia coli uvrD* gene encoding DNA helicase II. A biochemical and genetic characterization. J. Mol. Biol. 235, 424–435 (1994). https://doi.org/10.1006/jmbi.1994.1003
[46] Rasnik, I., Myong, S., Cheng, W., Lohman, T. M., Ha, T. DNA-binding orientation and domain conformation of the *E. coli* rep helicase monomer bound to a partial duplex junction: Single-molecule studies of fluorescently labeled enzymes. J. Mol. Biol. 336, 395–408 (2004). https://doi.org/10.1016/j.jmb.2003.12.031
[47] Arslan, S., Khafizov, R., Thomas, C. D., Chemla, Y. R., Ha, T. Engineering of a superhelicase through conformational control. Science 348, 344–347 (2015). https://doi.org/10.1126/science.aaa0445
[48] Makurath, M. A., Whitley, K. D., Nguyen, B., Lohman, T. M., Chemla, Y. R. Regulation of Rep helicase unwinding by an auto-inhibitory subdomain. Nucleic Acids Res. 47, 2523–2532 (2019). https://doi.org/10.1093/nar/gkz023
[49] Carney, S. P., Ma, W., Whitley, K. D., Jia, H., Lohman, T. M., Luthey-Schulten, Z., et al. Kinetic and structural mechanism for DNA unwinding by a non-hexameric helicase. Nat. Commun. 12, 7015 (2021). https://doi.org/10.1038/s41467-021-27304-6
[50] Marianayagam, N. J., Sunde, M., Matthews, J. M. The power of two: Protein dimerization in biology. Trends Biochem. Sci. 29, 618–625 (2004). https://doi.org/10.1016/j.tibs.2004.09.006
[51] Goodsell, D. S., Olson, A. J. Structural symmetry and protein function. Annu. Rev. Biophys. Biomol. Struct. 29, 105–153 (2000). https://doi.org/10.1146/annurev.biophys.29.1.105